

Lattice Boltzmann Model for Simulation of Avalanche Formation and Streamer Discharge in Breakdown of Gaseous Dielectrics

Nan Wang^{1,2} and Qingquan Lei¹

¹ College of Electrical & Electronic Engineering
Harbin University of Science Technology, Harbin 150080, P.R. China
51949083@qq.com, lei_qingquan@sina.com

² School of Mathematical Science
Heilongjiang University, Harbin 150080, P.R. China

Abstract — Gas discharges play a central role in the electrical breakdown of matter, both in nature and technology. Therefore, accurate modeling and simulation of streamers in gaseous discharge processes are of particular interest. This study presents the formulation of computationally efficient models of the charge density and electric field produced by the lattice Boltzmann method. The propagation of double-headed streamers is described in 1-cm plane-to-plane geometry in pure nitrogen at atmospheric pressure by 1.5D and 2D models. The lattice Boltzmann method was successfully applied to the simulation of streamer discharges. Therefore, this scheme is a potential way of simulating gaseous discharge problems.

Index Terms — Lattice Boltzmann method, numerical simulation, streamer discharge.

I. INTRODUCTION

The discharge phenomena in gaseous dielectrics have high practical importance. Knowledge of the discharge characteristics in gaseous dielectrics is important in solving several practical problems that arise in insulation systems. Completely revealing the mechanism of streamer discharges based on existing experiment strategies is impossible, and many important microcosmic physical quantities remain undetermined. Thus, numerical simulation has become an important method in advancing the development of gas discharge theory. Different models have been developed to study streamer propagation. However, a high-accuracy algorithm is required for the streamer discharge distribution of particles in large changes in space. Kunhardt and Min introduced the finite difference and finite element methods, respectively, to solve this model. Kunhardt presented results from a self-consistent, 2D numerical simulation of streamer formation and propagation in non-attaching (N_2) and attaching (N_2 - SF_6 mixture) gases using a one-moment

fluid model [1]. Min proposed the use of an adaptive mesh generation as a method of streamer simulation. A higher resolution and more efficient grid distribution with fewer grids can be obtained through adaptive mesh generation [2]. However, this method generally requires the Poisson and Boltzmann equations to be solved in each step, which make calculations complex and computer programs generally difficult to complete.

Describing charge density, electric-field distribution, temperature, and other physical quantities has been a major problem in simulating the streamer discharge development process by computer technology. 2D flux-corrected transport techniques are well-known and popular methods for the numerical calculation of streamer propagation. These methods allow for the numerical solution of transport equations under strongly space-charge-dominated conditions such as those that occur at the head of propagating streamers. Medvedev recently applied the lattice Boltzmann model (LBM) to simulate the electric breakdown in liquids and investigated pre-breakdown hydrodynamic flows and initial stages of the electric breakdown in dielectric liquids. These three models (the purely thermal, bubble, and combined models) were used to describe the expansion of streamer channels [3]. Kupershtokh developed an efficient lattice Boltzmann equation (LBE) model to simulate different electrohydrodynamic (EHD) phenomena. This model includes fluid dynamics, electric-charge transport through advection and conduction currents, and action of electric forces upon space charges in liquids [4]. The current study applies the LBE model for the numerical simulation of avalanche and streamers.

II. MODEL FORMULATION

A. Lattice Boltzmann model

The kinetic nature of LBM introduces three important features that distinguish it from other numerical methods. First, the convection operator (or

streaming process) of the LBM in phase space (or velocity space) is linear. This feature is borrowed from kinetic theory and contrasts with nonlinear convection terms in other approaches that use macroscopic representations. Simple convection combined with a relaxation process (or collision operator) allows the recovery of nonlinear macroscopic advection through multi-scale expansions. Second, incompressible Navier–Stokes (NS) equations can be obtained in the nearly incompressible limit of the LBM. The pressure in the LBM is calculated using an equation of state. By contrast, pressure satisfies a Poisson equation with velocity strains that act as sources in the direct numerical simulation of incompressible NS equations. Solving this equation for pressure often produces numerical difficulties that require special treatment such as iteration or relaxation. Third, the LBM utilizes a minimal set of velocities in phase space. The phase space is a complete functional space in traditional kinetic theory with the Maxwell–Boltzmann equilibrium distribution. The averaging process involves information from the entire velocity phase space. Given that only one or two speeds and a few moving directions are used in LBM, the transformation that relates to the microscopic distribution function and macroscopic quantities is simplified, which consists of simple arithmetic calculations.

The LBE can be obtained from either discrete velocity models or the Boltzmann kinetic equation, and deriving macroscopic NS equations from the LBE can be performed in several ways. This study uses an LBM model that begins from a discrete kinetic equation for the particle distribution function, which is commonly used [5-7]. Thus,

$$f_i(\mathbf{x} + e_i \Delta t, t + \Delta t) - f_i(\mathbf{x}, t) = \Omega_i(f_i(\mathbf{x}, t)), \quad (1)$$

where f_i is the particle velocity distribution function along the i -th direction, Δt is the time increment, e_i is the lattice direction velocity, and $\Omega_i(f_i(\mathbf{x}, t))$ is the collision operator that represents the change rate for f_i that results from collision:

$$\rho = \sum_i f_i \quad \rho \mathbf{u} = \sum_i f_i e_i, \quad (2)$$

where ρ is the density, and \mathbf{u} is the particle velocity.

This study uses the Bhatnagar–Gross–Krook (BGK) approximation as follows:

$$\Omega_i(f_i(\mathbf{x}, t)) = -(f_i - f_i^{eq}) / \tau, \quad (3)$$

where τ is a single relaxation time parameter. In the BGK model, relaxation time τ governs transport coefficients such as viscosity, heat conductivity, and diffusivity, and is expressed as:

$$\tau = 3\nu \frac{\Delta t}{\Delta x^2} + 0.5, \quad (4)$$

where ν is the kinematics viscosity of fluid, Δx is the lattice length, and f_i^{eq} in Equation (3) is the equilibrium distribution function. The equilibrium distribution

function can be analytically obtained [8]:

$$f_i^{eq} = \omega_i \rho \left(1 + \frac{e_i \cdot \mathbf{u}}{c_s^2} + \frac{(e_i \cdot \mathbf{u})^2}{2c_s^4} - \frac{\mathbf{u}^2}{2c_s^2} \right). \quad (5)$$

At this point, we consider the following 2D model with nine velocities:

$$e_i = \begin{cases} (0, 0), & i=0 \\ \left(\cos\left(\frac{(i-1)\pi}{2}\right), \sin\left(\frac{(i-1)\pi}{2}\right) \right), & i=1, 2, 3, 4 \\ \left(\cos\left(\frac{(i-5)\pi}{2} + \frac{\pi}{4}\right), \sin\left(\frac{(i-5)\pi}{2} + \frac{\pi}{4}\right) \right), & i=5, 6, 7, 8 \end{cases} \quad (6)$$

The direction of e_i is shown in Fig. 1 for the nine-velocity model.

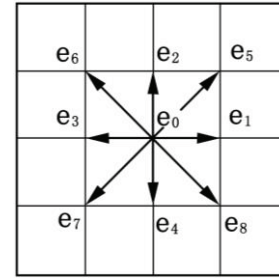


Fig. 1. Lattice velocities for the 2D model.

In Equation (5), ω_i is the weight coefficient, $\omega_0 = 4/9$, $\omega_1 = \omega_2 = \omega_3 = \omega_4 = 4/9$, $\omega_5 = \omega_6 = \omega_7 = \omega_8 = 1/36$, and c_s is the sound speed expressed as:

$$c_s = \sqrt{RT} = 1/\sqrt{3}. \quad (7)$$

This study uses the lattice Boltzmann method to solve equations for the concentrations of electric charge carriers. We considered a new gravity model in the lattice Boltzmann method for charged particle transport forced by an electric field. When a body force is included in the Boltzmann equation, expressing force in terms of its gravitational potential ($-\rho \nabla \phi$) is common. If this approach is considered and the density variation produced by the body force is negligible, the Boltzmann equation that incorporates the body force can be expressed in the same form as in the absence of gravity but with an altered pressure ($p \rightarrow p + \rho \phi$). If a gravitational force \mathbf{F} acts, then a change in momentum $\Delta p = \mathbf{F}$ at every time step occurs. This condition was incorporated into a model of equilibrium distribution [9,10]. Thus,

$$\Omega_i(f_i(\mathbf{x}, t)) = -(f_i - f_i^{eq}) / \tau + \Delta t F_i, \quad (8)$$

where

$$F_i = \omega_i \left(1 - \frac{1}{2\tau} \right) \frac{e_i \cdot \mathbf{F}}{c_s^2}. \quad (9)$$

B. LBM model for avalanche

A key problem encountered in the breakdown

simulation is the establishment of the electron avalanche. A numerical simulation of an electron avalanche generally adopts the random Monte Carlo algorithm. However, the form of an electron avalanche and contact between the breakdown field strength and process cannot be reflected properly with this method. This study presents a simulation of the signal development of an electron avalanche using a transport model based on Boltzmann equations.

The electron avalanche formation process was described to simulate this breakdown, and the number of electrons can be expressed using the following equation:

$$n = \alpha dx, \quad (10)$$

where n is the number of newly generated electrons produced by collision, α is the ionization coefficient, and dx is the distance of an electron avalanche. We assume that the n_0 electron at the negative electrode causes an electron avalanche breakdown by impact ionization under the action of the breakdown strength. Thus,

$$n = n_0 \exp \int_0^x \alpha dx. \quad (11)$$

This study uses a 2D nine-velocity D2Q9 model to describe the breakdown evolution process [9,11]. Positive ions and electrons were mainly considered to describe the initial electron avalanche formation process:

$$n = n_e = \rho_e, \quad n_p = \rho_p, \quad (12)$$

$$\rho_e = \sum_i f_{e_i}, \quad \rho_p = \sum_i f_{p_i}. \quad (13)$$

The expression for the charge density distribution function is as follows:

$$f_i(x+e_i\Delta t, t+\Delta t) = (\alpha_i - \eta_i) f_i(x, t) + \frac{f_i^{eq}(\rho_e + \rho_p, u) - f_i(x, t)}{\tau}, \quad (14)$$

where e_i is the direction vector of the electron. In the following 2D nine-velocity D2Q9 model:

$$e_i = \begin{bmatrix} 0 & 1 & 0 & -1 & 0 & 1 & -1 & -1 & 1 \\ 0 & 0 & 1 & 0 & -1 & 1 & 1 & -1 & -1 \end{bmatrix}, \quad (15)$$

α_i is the impact ionization coefficient, which is related to the electric field and particle mobility velocity. Electron and positive ion velocities can be written as the electron and positive ion mobilities that multiply the electric field, respectively.

The discharge process is transient, so the Poisson equation and particle transport equation should be solved at each step. For a given charge distribution, the electric field can be calculated by the charge intensity. The impact ionization coefficient and particle velocity can then be calculated by the local field. Furthermore, next-step charge distribution can be calculated by previous step parameters.

C. Simulation for streamer discharges

For streamer simulations in nitrogen at atmospheric pressure, the following standard drift-diffusion equations were used for electrons, positive ions, and anion, which were coupled to the Poisson equation:

$$\begin{cases} \frac{\partial n_e}{\partial t} + \nabla \cdot (v_e n_e) = \nabla^2 (D n_e) + (\alpha - \eta) n_e + |v_e| + s \\ \frac{\partial n_p}{\partial t} + \nabla \cdot (v_p n_p) = \alpha n_e + |v_e| + s \\ \frac{\partial n_n}{\partial t} + \nabla \cdot (v_n n_n) = \eta n_e + |v_e| \\ \nabla \cdot (\varepsilon \nabla U) = -e(n_p - n_n - n_e) \\ E = -\nabla U \end{cases}, \quad (16)$$

where n_e and n_p are electron and positive ion densities, respectively, n_n is the anion density, $v_i = u_i E$ is the drift velocity of electrons, E is the electric field, and u_i is the electron mobility. D is the electron diffusion coefficient, and α represents the impact ionization coefficient. U is the electric potential, s is the photoionization, ε is the permittivity of free space, and e is the electron charge [12, 13].

Considering the photoionization process in a numerical simulation is important. The photoionization model developed by Zhelezniak was introduced into the numerical simulation of streamer discharge in atmospheric air [14,15]. Given the non-locality of radiative transfer, the photoionization model involves describing radiative relations between all points of the plasma. Thus, calculating the photoionization model is complex. A model derived by Zheleznyak is an example of photoionization in air, where the photoionization rate at the point of observation \mathbf{r} because of source points of emitting photoionizing UV photons at \mathbf{r}' is as follows:

$$S = \iiint_D \frac{I(\mathbf{r}') f(R)}{4\pi R^2} dD, \quad (17)$$

where $R = |\mathbf{r} - \mathbf{r}'|$. The photon production in this model is assumed to be proportional to the ionization production rate S_i , and $I(\mathbf{r})$ is given by the following:

$$I(\mathbf{r}) = \xi \frac{n_u(\mathbf{r}')}{\tau_u} = \frac{p_q}{p + p_q} \xi \frac{v_u}{v_i} S_i(\mathbf{r}), \quad (18)$$

where ξ is the photoionization efficiency, $n_u(\mathbf{r})$ is the density of \mathbf{u} , the ratio $p_q/(p+p_q)$ is a quenching factor, τ_u is the lifetime of the excited state \mathbf{u} that accounts for the effects of spontaneous emission and quenching, v_u is the electron impact excitation frequency for level \mathbf{u} , and $S_i = v_i n_e$ (where n_e is the electron number density and v_i is the ionization frequency). The function $f(R)$ in Equation (17) is defined in two studies [16-18].

The distribution function and charge density were used in the present study to describe photoionization. In a traditional LBM model, Ω_i is required to satisfy the conservation of the total mass and total momentum at each lattice as follows:

$$\sum_i \Omega_i = 0, \quad \sum_i \Omega_i e_i = 0. \quad (19)$$

The sum of all collision operators Ω_i in our model is equal to photoionization:

$$\sum_i \Omega_i = S, \quad \sum_i \Omega_i e_i = S \mathbf{u}. \quad (20)$$

If only the physics in long wavelengths and low-frequency limits are important, the lattice spacing Δx and time increment Δt in Equation (1) can be regarded as small parameters of the same order ε . Through a Taylor expansion in time and space, the following continuum form of the kinetic equation accurate to the second order in ε can be obtained:

$$\frac{\partial f_i}{\partial t} + e_i \cdot \nabla f_i + \varepsilon \left(\frac{1}{2} e_i^2 \cdot \nabla^2 f_i + e_i \cdot \nabla \frac{\partial f_i}{\partial t} + \frac{1}{2} \frac{\partial^2 f_i}{\partial t^2} \right) = \frac{\Omega_i}{\varepsilon}. \quad (21)$$

The Chapman–Enskog expansion can be employed to derive the macroscopic hydrodynamic equation, which is essentially a formal multi-scaling expansion:

$$\begin{cases} \frac{\partial}{\partial t} = \varepsilon \frac{\partial}{\partial t_1} + \varepsilon^2 \frac{\partial}{\partial t_2} \\ \frac{\partial}{\partial x} = \varepsilon \frac{\partial}{\partial x_1} \end{cases}. \quad (22)$$

The Equation (22) assumes that the diffusion time scale t_2 is much slower than the convection time scale t_1 . The one-particle distribution function f_i can similarly be expanded formally on the local equilibrium distribution function f_i^{eq} and photoionization distribution function f_i^{seq} :

$$f_i = f_i^{eq} + f_i^{seq} + \varepsilon (f_i^{neq}). \quad (23)$$

At this point, f_i^{eq} depends on the local macroscopic variables (ρ and $\rho \mathbf{u}$) and should satisfy the following constraints:

$$\sum_i f_i^{eq} = \rho, \quad \sum_i f_i^{eq} e_i = \rho \mathbf{u}. \quad (24)$$

f_i^{seq} depends on the local macroscopic variables (S and $S \mathbf{u}$) and should satisfy the following constraints:

$$\sum_i f_i^{seq} = S, \quad \sum_i f_i^{seq} e_i = S \mathbf{u}. \quad (25)$$

Thus,

$$f_i^{neq} = f_i^{(1)} + \varepsilon f_i^{(2)} + O(\varepsilon^2), \quad (26)$$

is the non-equilibrium distribution function, which has the following constraints:

$$\sum_i f_i^{(k)} = 0, \quad \sum_i f_i^{(k)} e_i = 0, \quad (27)$$

for both $k = 1$ and $k = 2$. When f_i is inserted into the collision operator Ω_i , the Taylor expansion provides the following:

$$\Omega_i = \Omega_i(f_i^{eq}) + \Omega_i(f_i^{seq}) + O(\varepsilon^3). \quad (28)$$

From Equation (21), we note that when $\varepsilon \rightarrow 0$, then $\Omega_i(f_i^{eq}) = 0$, $\Omega_i(f_i^{seq}) = S$. This condition leads to the following linearized collision operator:

$$\frac{\Omega_i}{\varepsilon} = \frac{M_{ij}}{\varepsilon} (f_i - f_i^{eq} - f_i^{seq}), \quad (29)$$

where

$$M_{ij} = \frac{\partial \Omega_i(f_i^{eq})}{\partial f_j}, \quad (30)$$

is the collision matrix that determines the scattering rate between directions i and j . For a given lattice, M_{ij} only depends on the angle between directions i and j , and has a limited set of values. For mass and momentum conservation collision, M_{ij} satisfies the following constraints [19]:

$$\sum_i M_{ij} = 0, \quad \sum_i M_{ij} e_i = 0. \quad (31)$$

If we further assume that the local particle distribution relaxes to an equilibrium state at a single rate:

$$M_{ij} = -\frac{1}{\tau} \delta_{ij}, \quad (32)$$

we then arrive at the lattice BGK (LBGK) collision term [20]:

$$\frac{\Omega_i}{\varepsilon} = \frac{1}{\tau} (f_i^{seq} - f_i^{neq}) = \frac{1}{\tau} f_i^{seq} - \frac{1}{\varepsilon \tau} (f_i^{(1)} + f_i^{(2)}), \quad (33)$$

and the LBGK equation:

$$f_i(\mathbf{x} + e_i \Delta t, t + \Delta t) - f_i(\mathbf{x}, t) = -\frac{f_i - f_i^{eq} - f_i^{seq}}{\tau}. \quad (34)$$

Photoionization is described at this point by the equilibrium distribution function from an LBGK model:

$$f_i^{seq} = E_i(S, \mathbf{u}) = \omega_i S \left(1 + \frac{e_i \cdot \mathbf{u}}{c_s^2} + \frac{(e_i \cdot \mathbf{u})^2}{2c_s^4} - \frac{u^2}{2c_s^2} \right). \quad (35)$$

Finally, the LBM equation for streamer discharge simulation is written as follows:

$$f_i(\mathbf{x} + e_i \Delta t, t + \Delta t) - f_i(\mathbf{x}, t) = -\frac{f_i - f_i^{eq} - f_i^{seq}}{\tau} + \Delta t F_i. \quad (36)$$

D. Numerical algorithm processes

The solution procedure can be illustrated by the following numerical algorithms:

- Initial equilibrium distribution function $f_i(\mathbf{x}, 0)$;
- Poisson's equation and algorithm for the electric field force and photoionization are solved;
- Continuity equations are computed as follows:

$$f_i'(\mathbf{x}, t) = f_i(\mathbf{x}, t) + \frac{f_i - f_i^{eq} - f_i^{seq}}{\tau} + \Delta t F_i; \quad (37)$$

- Migration for location is executed as follows:

$$f_i(\mathbf{x} + e_i \Delta t, t + \Delta t) = f_i'(\mathbf{x}, t); \quad (38)$$

- Macroscopic quantities are computed as follows:

$$\rho(\mathbf{x}, t + \Delta t) = \sum_{i=1} f_i(\mathbf{x}, t + \Delta t), \quad (39)$$

$$\rho \mathbf{u}(\mathbf{x}, t + \Delta t) = \sum_{i=1} f_i e_i(\mathbf{x}, t + \Delta t); \quad (40)$$

(f) If $t + \Delta t < t_{\text{final}}$, then step (b) is repeated.

III. NUMERICAL RESULTS

A. Numerical results of an electron avalanche

This section first investigates the physical quantity of electron density, which depicts the process of an electron avalanche. The computational domain is 256×256 , and the characteristic is $L = 256$, $\Delta x = 1$. The electric breakdown of gas that occurs in a uniform electric field is directed vertically. We used periodic boundary conditions at the sides of the computation area and solid walls at the top and bottom. Charge injection from the tip results in the formation of an electron avalanche. As the conductive channel reaches the second electrode, the channel stage of the electric breakdown begins. Simulation results are shown in Fig. 2.

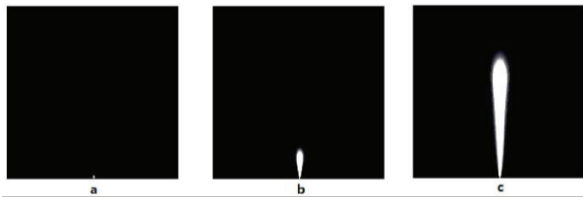


Fig. 2. Growth of an electron avalanche channel. Time at: (a) $t = 10$, (b) $t = 200$, and (c) $t = 1000$. The white color corresponds to the electron density.

Figure 3 shows an initial electron avalanche in the ionization chamber, which was obtained from a study [21]. The shape of the electron avalanche has a rough vertebral shape. Comparing Figs. 2 and 3 shows a remarkable similarity in the shape of the electron avalanche. Therefore, the result of using an LBE simulation is valid. The numerical simulation method is feasible at least for describing the shape of an electron avalanche.

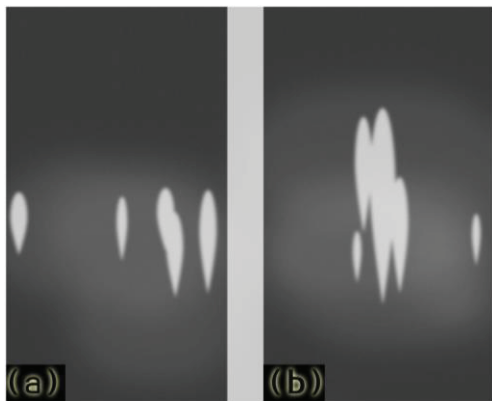


Fig. 3. Initial electron avalanche in the ionization chamber is shown. $P = 270$ (133 Pa), $E = 10.5$ kV/cm.

B. Propagation of a 1.5D model for streamer discharges

The following section attempts to demonstrate the efficiency of using an LBM model for the two examples selected among classic streamer simulation test cases. First, a 1.5D model was used. The numerical solutions of these equations have been limited to simple situations for a long time, in which the streamer was assumed to be confined inside a cylinder with a constant radius. Inside the cylinder, the charged particle density was assumed to be confined inside a cylinder with a constant radius and constant along the radial direction. The space and time evolution of charged particles can only be calculated in one dimension (along the direction of propagation) under these conditions, and the electric field was obtained using the so-called disc method. If only a 1D approach is necessary to calculate the space and time variations of charged particle densities, noting that the electric field has to be calculated in two dimensions is important. This approach is recognized in 1.5D model studies, and was popular during the early stages of streamer simulation. At present, this approach is mainly used to rapidly check the accuracy of different numerical models. Thus, the 1.5D model was used in the subsequent sections for the said purpose. Second, the complete 2D propagation of a double-headed streamer under a homogeneous electric field was investigated. These results allow us to check the efficiency of the LBM in different scenarios and demonstrate strong improvements compared with other models. Calculations were made using the 1.5D approximation defined in the previous section, and the propagation of a double-headed streamer was calculated by an LBM Q1D3 model. The propagation of a double-headed streamer was considered in plane-to-plane geometry in pure nitrogen at atmospheric pressure [22]. The cathode is located at $x = 1$ and the anode is located at $x = 0$. The applied voltage is equal to 52 kV. A 0.05 cm discharge radius was selected. The initial distribution of electrons and ions has the following Gaussian shape:

$$n_e(x, 0) = n_p(x, 0) = n_b + n_0 \left(\exp\left(-\frac{(x-x_0)^2}{\sigma_x}\right) \right), \quad (41)$$

with $\sigma_x = 0.027$ cm, $x_0 = 0.5$ cm, $n_0 = 10^{14}$ cm³, and $n_b = 10^8$ cm³. Two streamers start to propagate toward the opposite electrodes in this case.

Figures 4 and 5 reveal the space variation of the net charge density and electric field during double-headed streamer propagation. Figure 4 shows the comparison of charge densities at four different time points ($t = 0.5, 1.5, 2.5, 3$ ns) during streamer head propagation. Figure 5 shows the comparison of the electric field at four different time points ($t = 0.5, 1.5, 2.5, 3$ ns) during streamer head propagation. After 2.5 ns of propagation, the propagation distance of the anode-directed streamer

is 1.8 cm, whereas that of the cathode-directed streamer is 2.8 cm. The velocity of the anode-directed streamer is 0.8×10^8 cm/s to 1.8×10^8 cm/s, whereas that of the cathode-directed streamer is 0.4×10^8 cm/s to 1.0×10^8 cm/s. Two regions have large charge densities on the head of the double-headed streamer. These results are similar to the findings of a previous study [23].

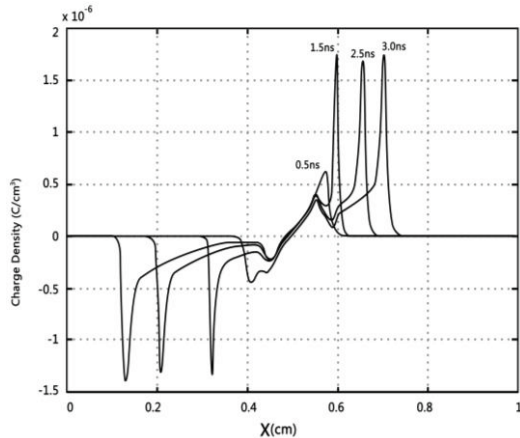


Fig. 4. Double-headed streamer front propagation and charge density at different time points ($t = 0.5, 1.5, 2.5, 3$ ns) are shown.

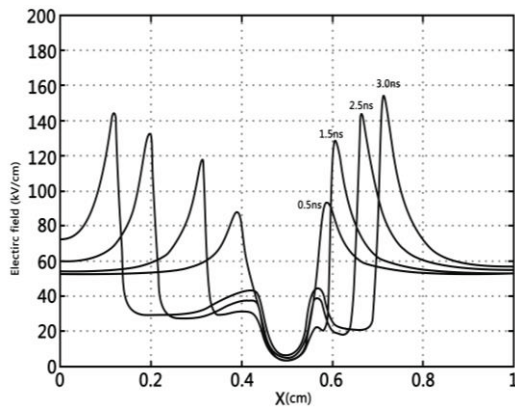


Fig. 5. Double-headed streamer front propagation and electric field at different time points ($t = 0.5, 1.5, 2.5, 3$ ns) are shown.

C. Propagation of 2D double-headed streamer

Calculations in this section were performed using the 2D approximation defined in the previous section, and the propagation of a double-headed streamer was calculated using the LBM Q2D9 model. The size of the computational domain is 1.4×0.125 cm². The center of the Gaussian distribution is located in the middle of the simulation domain at $x_0 = 0.7$ cm. The applied voltage is equal to 52 kV. Figure 6 shows a cross-sectional

view of the charge density distributions and electric field at $t = 3.0$ ns, which was obtained using the Q2D9 LBM model. This cross-sectional view represents an example of the 2D views of the simulation results. The streamer propagation under homogeneous electric fields validates the effectiveness of the LBM model compared with other computational models [24,25].

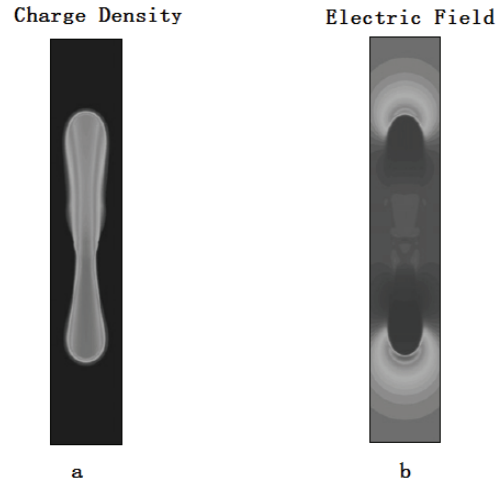


Fig. 6. Propagation of a double-headed streamer in a 2D domain and a cross-sectional view of distributions of the: (a) charge density and (b) electric field at $t = 3.0$ ns.

IV. DISCUSSION AND CONCLUSION

This study attempted to simulate the gaseous discharge process using an LBM model. The LBM model has been developed into an alternative and promising scheme for different types of numerical simulations in recent years. Unlike other numerical schemes, the lattice Boltzmann method was based on microscopic models and mesoscopic kinetic equations. This scheme can be particularly successful in fluid flow applications and numerical simulations of EHD problems. This study is only an experimental application of the LBM, which was applied to break down gaseous dielectric problems. We have also compared the LBM streamer model with other results obtained using different numerical techniques to solve transport equations for charged particles. The efficiency of the LBM was supported by similar results. Several issues remained unsolved in this model, such as the use of simple photoionization. In addition, the LBM model has several unique advantages on the complex boundary problem and porous material issues. Combined with the theory of discharge gas systems and characteristic advantage of this model, several gas discharge conditions at the complex boundary were examined. This study can be an important reference for solving several practical problems in the future.

ACKNOWLEDGMENT

This research was supported by the Major Research Plan of the National Natural Science Foundation of China (2012CB723308), and the Science Technology Research Program of the Heilongjiang Educational Committee (12541611).

REFERENCES

- [1] C. Wu and E. Kunhardt, "Formation and propagation of streamers in N_2 and N_2 - SF_6 mixtures," *Physical Review A*, vol. 37, no. 11, pp. 4396-4406, Jun. 1988.
- [2] G. E. Georghiou, et. al., "Numerical modelling of atmospheric pressure gas discharges leading to plasma production," *Journal of Physics D Applied Physics*, vol. 38, no. 20, pp. 303-328, Sep. 2005.
- [3] D. A. Medvedev, "Lattice Boltzmann model for simulation of the electric breakdown in liquids," *Procedia Computer Science I*, vol. 1, no. 1, pp. 811-818, Apr. 2010.
- [4] A. L. Kupershtokh, "Lattice Boltzmann equation method in electrohydrodynamic problems," *Journal of Electrostatics*, vol. 64, no. 7-9, pp. 581-585, Nov. 2006.
- [5] H. Huang, L. Wang, and X-Y. Lu, "Evaluation of three lattice Boltzmann models for multiphase flows in porous media," *Computers and Mathematics with Applications*, vol. 61, no. 12, pp. 3606-3617, 2011.
- [6] Y. L. He and Y. Wang, *Lattice Boltzmann Method Theory and Application*, Science Press, China, 2009.
- [7] S. Chen and G. D. Doolen, "Lattice Boltzmann method for fluid flows," *Annu. Rev. Fluid Mech.*, vol. 30, no. 5, pp. 329-364, Aug. 1998.
- [8] Y. Qian and D. d'Humieres, "Lattice BGK models for Navier-Stokes equation," *Europhys*, vol. 17, no. 6, pp. 479-484, Jan. 1992.
- [9] Z. Li. Guo and C. G. Zheng, *Theory and Application of Lattice Boltzmann Method*, Science Press, China, 2009.
- [10] J. M. Buick and C. A. Greated, "Gravity in a lattice Boltzmann model," *Physical Review E*, vol. 61, no. 5, pp. 5307-5320, May 2000.
- [11] N. Wang, Q. Lei, and X. Wang, "Lattice Boltzmann model for simulation of the electric charge flow and calculation of electrorheology," *International Journal of Digital Content Technology and its Applications*, vol. 6, no. 17, pp. 135-143, Sep. 2012.
- [12] L. B. Loeb and J. M. Meek, "The mechanism of spark discharge in air at atmospheric pressure," *J. Appl. Phys*, vol. 11, no. 6, pp. 438-47, Nov. 1940.
- [13] A. J. Davies and C. S. Davies, "Computer simulation of rapidly developing gaseous discharges," *PROC. IEE.*, vol. 118, no. 6, pp. 816-823, 1971.
- [14] M. B. Zheleznyak, A. K. Mnatsakanian, S. V. Sizykh, "Photoionization of nitrogen and oxygen mixtures by radiation from gas discharge," *High Temperature*, vol. 20, no. 3, pp. 357-362, 1982.
- [15] J. Roger-Riba, P. Casals-Torrens, and R. Bosch, "Defects identification in XLPE medium-voltage cables by applying multivariate methods," *DYNA*, vol. 89, no. 6, pp. 633-641, 2014.
- [16] G. W. Penney and G. T. Hummert, "Photoionization measurements in air oxygen and nitrogen," *Journal of Applied Physics*, vol. 41, no. 2, pp. 572-577, Aug. 1970.
- [17] A Bourdon, et. al., "Efficient models for photoionization produced by non-thermal gas discharges in air based on radiative transfer and the Helmholtz equations," *Plasma Sources Science and Technology*, vol. 16, no. 3, pp. 656-678, Aug. 2007.
- [18] W. J. Yao and S. P. Chen, "Elastic-plastic analytical solutions of deformation of uplift belled pile," *Tehnicki Vjesnik-Technical Gazette*, vol. 21, no. 6, pp. 1201-1211, Dec. 2014.
- [19] R. Benzi, S. Succi, M. Vergassola, "The lattice Boltzmann equation theory and applications," *Phys. Rep.*, vol. 222, no. 3, pp. 145-97, 1992.
- [20] P. L. Bhatnagar, E. P. Gross, and M. Krook, "A model for collision processes in gases: small amplitude processes in charged and neutral one component system," *Phys. Rev.*, vol. 94, no. 3, pp. 511-525, Jan. 1955.
- [21] Y. Zhang, *High Voltage and Insulation Technology*, China Power Press, Beijing, 2002.
- [22] A. Boretti and S. Jiang, "Development of a two stroke direct injection jet ignition compressed natural gas engine," *Journal of Power Technologies*, vol. 94, no. 3, pp. 145-152, Mar. 2014.
- [23] D. Bessieres, J. Paillol, A. Bourdon, and P. Segur, "A new one-dimensional moving mesh method applied to the simulation of streamer discharges," *Journal of Physics D: Applied Physics*, vol. 40, no. 21, pp. 6559-6570, Apr. 2007.
- [24] C. Zhuang and R. Zeng, "Discountinuous Galerkin method for short air gap discharge simulations and its applications," *High Voltage Engineering*, vol. 39, no. 4, pp. 970-978, Apr. 2013.
- [25] Y. Zhang and R. Zeng, X-C. Yang, and B. Zhang, "Study on photoionization produced by discharge in atmospheric air by numerical method," *Proceedings of the CSEE*, vol. 29, no. 4, pp. 110-116, Feb. 2009.



Nan Wang (1984.5-), male, native place: Harbin in China, Ph.D. Student of the Harbin University of Science Technology, working in the School of Mathematical Science of Heilongjiang University. Research focus: lattice Boltzmann and high-voltage insulation.



Qingquan Lei (1938.7-), male, native place: Sichuan Province in China, Academician of the Engineering Academy, and Professor of the Harbin University of Science Technology. Research focus: high voltage and insulation techniques.